PASJ: Publ. Astron. Soc. Japan , 1–??,
© 2010. Astronomical Society of Japan.

arXiv:1002.3656v1 [astro-ph.SR] 19 Feb 2010

Spectroscopic Studies of Limb Spicules.
I. Radial and Turbulent Velocities

Makiko Shoji, Takara Nishikawa
Kyoto College of Economics, 3-1 Higashinaga-cho Ooe, Nishikyo-ku, Kyoto, 610-1195
shoji@kyoto-econ.ac.jp, nishikawa@kyoto-econ.ac.jp
Reizaburo Kitai
Kwasan Observatory, Graduate School of Science, Kyoto University,
17 Ohmine-cho Kita Kazan, Yamashina-ku, Kyoto, 607-8471
and
Satoru Ueno
Hida Observatory, Graduate School of Science, Kyoto University,
Kurabashira, Kamitakara-cho, Takayama, Gifu, 506-1314

(Received 2009 May 12; accepted 2010 January 5)

Abstract

We made high-resolution spectroscopic observations of limb-spicules in Hα using the Vertical Spectrograph of Domeless Solar Telescope at Hida Observatory. While more than half of the observed spicules have Gaussian line-profiles, some spicules have distinctly asymmetric profiles which can be fitted with two Gaussian components. The faster of these components has radial velocities of 10–40 km s^{-1} and Doppler-widths of $\sim$0.4 Å which suggest that it is from a single spicule oriented nearly along the line-of-sight. Profiles of the slower components and the single-Gaussian type show very similar characteristics. Their radial velocities are less than 10 km s^{-1} and the Doppler-widths are 0.6–0.9 Å. Non-thermal "macroturbulent" velocities of order 30 km s^{-1} are required to explain these width-values.

Key words: line:profiles — Sun:chromosphere — Sun:spicules

1. Introduction

Spicules are one of the fundamental elements of the quiet solar chromosphere, so it is important to know the physical properties of spicules to understand the quiet Sun. Pasachoff, Noyes, Beckers (1968) did a pioneering observation of limb spicules with many chromospheric emission lines, and derived the basic morphological and spectroscopic properties. They also suggested the rotation of spicule gas from the inclined spectra. Krat & Krat (1971) also made spectroscopic observations of limb spicules in 5 spectral lines, and reported that emission-line profiles are classified into narrow ones and wide ones. However, they were not sure whether they observed single individual spicules, since the spatial resolution of their study was several arcseconds. Summarizing these observational works, Beckers (1972) reviewed the morphology and spectroscopic properties of spicules and summarized that a spicule has a diameter of 400–1500 km and mean Doppler velocity of 10 km s^{-1}. Kulidzanishvili & Nikolsky (1978) observed 650 Hα line profiles of 25 spicules, and categorized them into two groups. One group is of relatively small intensity and narrow emission profiles, and the other is of brighter and wider ones. The characteristics of the latter group was thought to be due to the overlapping of unresolved spicules. They suggested that the Hα spicules have temperature of 6000 K and non-thermal velocities of $\sim$25 km s^{-1}. Follow-up spectroscopic observations of limb spicules under much better seeing conditions were done by Kulidzanishvili (1980) with the 53-cm Lyot coronagraph of Abastumani Astrophysical Observatory and by Hasan & Keil (1984) with Sacramento Peak VTT. From the study of line-of-sight (LOS) velocity and line-width distribution along the axis of spicules, they got a result that, in majority of spicules, the Hα line-width does not change spatially along the axes of spicules. Kulidzanishvili (1980) suggested that the line width of the majority of spicules are due to the overlapping of gas moving with relative velocities of 20–30 km s^{-1}.

Nishikawa (1988) used Hα filtergrams to determine the diameter and the motion of limb spicules. This morphological study found that the speed of the apparent up-and-down motion of large spicules is $\sim$50 km s^{-1}. Assuming ballistic motion, he estimated the initial velocity to be around 100 km s^{-1}, though there has been no other report of such high velocities. The typical diameter of spicules was about 500 km, although the best images show thinner components of 200 and 350 km in diameter.

Recent studies using Ca II H filtergram from Hinode has shown that spicules move more dynamically and have much smaller diameters than previously thought. De Pontieu et al. (2007b) found that the apparent maximum velocity of "type I" spicules is 15–35 km s^{-1}, and the apparent upward velocity of "Type II" spicules is 40–300 km s^{-1}. Suematsu et al. (2008) reported that a spicule consists of highly dynamic multi-threads as thin as a few tenths of an arcseconds and shows lateral movement or oscillation with rotation.

Although Hinode's direct imaging provides us highly valuable images, we need spectroscopic observations of spicules with high spatial and temporal resolutions to know the actual physical state of the spicular gas. As Sterling (1998) pointed out, knowledge of the actual physical properties is essential to theoretically clarify the dynamics and ejection process of spicules with numerical simulations. Recently, Pasachoff, Jacobson, Sterling (2009) presented the ground-based observations with very high spatial resolution done at the Swedish 1-m Solar Telescope on La Palma. They analyzed the imaging observations at five wavelengths around Hα. Although their observation provides us a new statistics on morphological and dynamical properties of limb spicules, they have derived the spectroscopic quantities such as LOS velocities under the rather simplified assumption of the Gaussian emission profiles. At present, further analyses of full line profiles in detail remain to be done to find the thermodynamical properties of spicular gas.

In our series of papers, we present the analyses of spectroscopic observations of limb spicules in Hα with high spatial resolution, which is comparable to the best resolution of ground-based observations. This paper reports and discusses the line widths and the radial velocities of spicules derived from our spectral images.

2. Observation

The observations were made on September 8, 2005 at Hida Observatory, using the Vertical Spectrograph of the Domeless Solar Telescope. The 3rd order spectra gave us the dispersion of 0.300 Å mm^{-1} and the spectral resolution 0.0123 Å (which corresponds 0.56 km s^{-1}) with the slit width 0.1 mm. Hα spectra were taken by Kodak Megaplus 1.6i CCD camera with 150 msec exposure time. The slit position was fixed during each series of observations and the camera continuously took the spectral images with a 1 sec time cadence.

We targeted the north polar limb which was covered by a large coronal hole at that time (figure 1). The slit was positioned parallel to the limb and at the tops of the spicules to get the optically thin profiles (figure 2). We were able to obtain more than 3500 frames of Hα spectral images with high spatial resolution during two series of observations around 01 UT and 06 UT. The height of the slit position at the nearest point from the solar limb seen in Hα+0.9 Å was 4200 km for 01 UT and 3700 km for 06 UT.

Among the numerous spectral images, we first discarded the frames showing dark lane of self-absorption around the Hα line center, since their profiles with flat-bottomed dip require the radiative transfer analysis to interpret and we wish to concentrate our profile analysis to optically thin emissions. Then, we further searched the frames showing good spatial resolution. As a result, seven frames shown in figure 3 were picked up for analysis, three from the sequence around 01 UT and four from 06 UT. The spatial FWHM values of the sharp streaks measured at ±0.8 Å are 1000–1900 km.

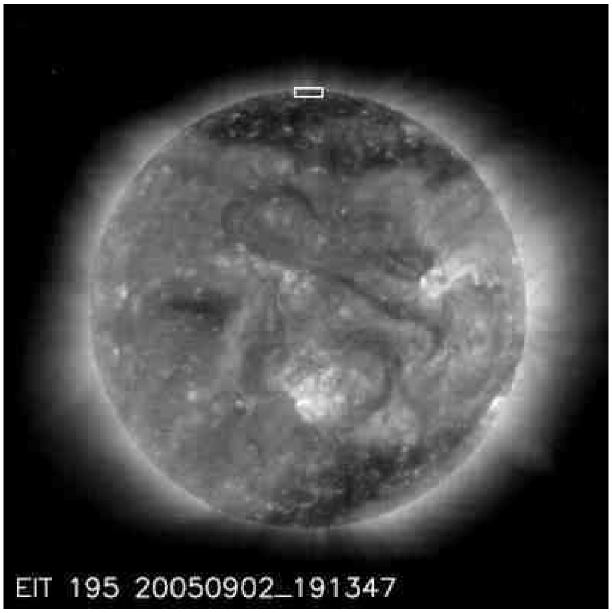

Fig. 1. SOHO EIT shows a coronal hole around the north pole. The rectangle indicates the observed region.

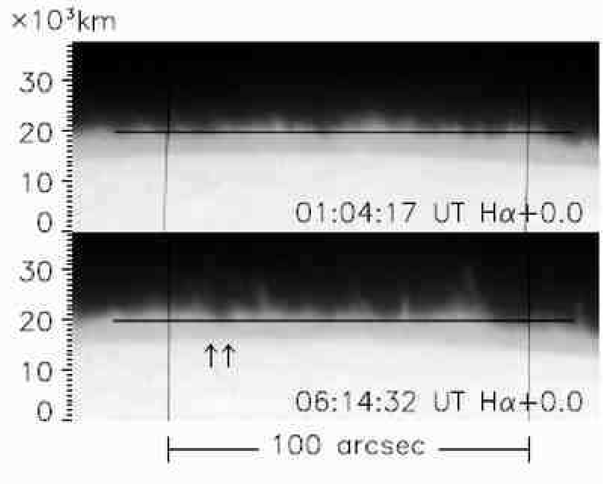

Fig. 2. Hα images of the observed regions at 01 UT and 06 UT. The horizontal line is the spectrograph slit. Two vertical lines are fiducial hairlines. The images are presented in logarithmic intensity scale to enhance the details around the slit. The arrows indicate the positions of two exceptional events mentioned in section 5.

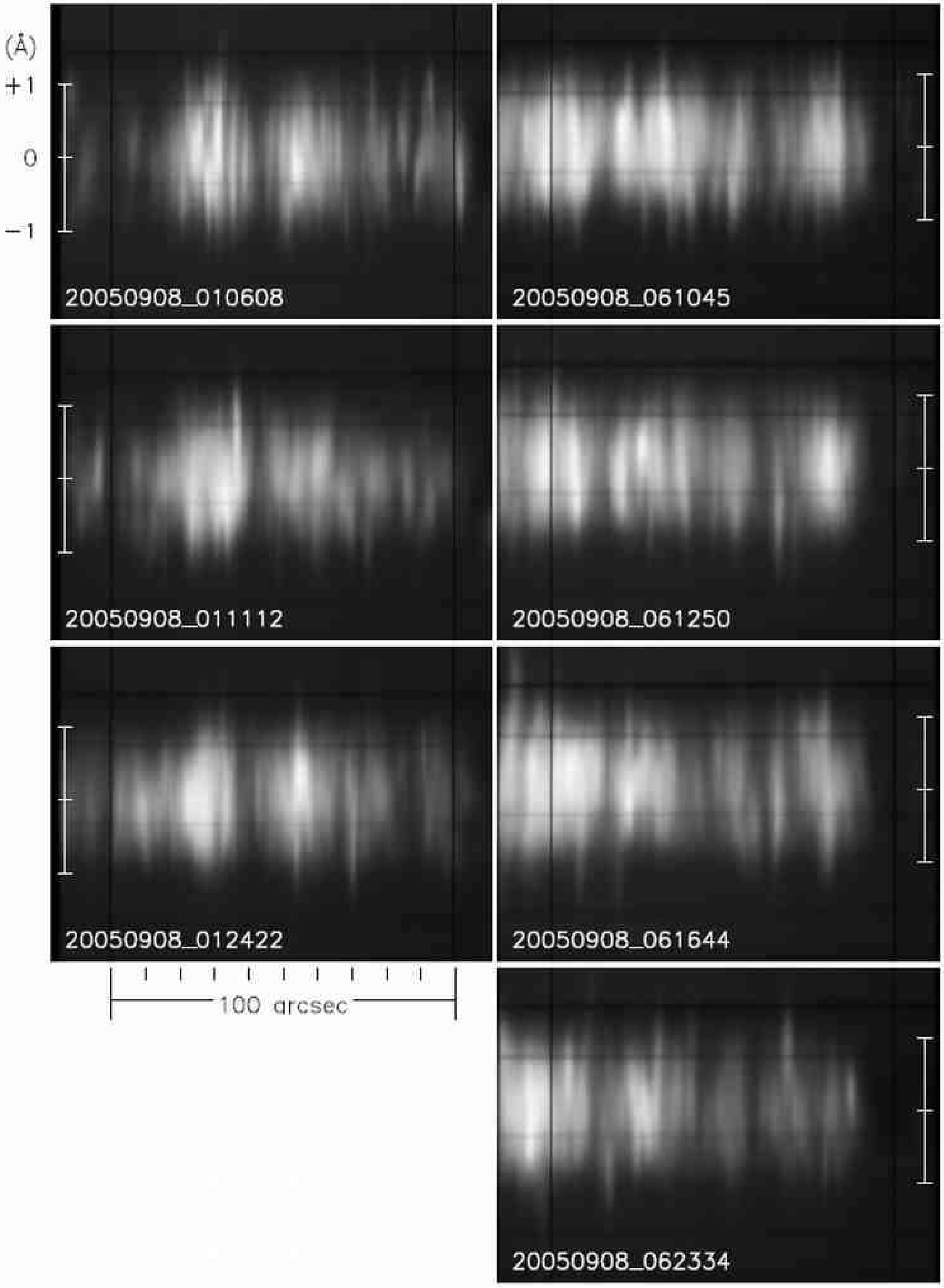

Fig. 3. Hα spectra of spicules analyzed in this paper. Two vertical lines correspond to the fiducial hairlines.

Recent Hinode/SOT observations found that the spatial widths of spicules are around 200 km or less. The spatial resolution of our spectroscopic observation is much coarser than the true widths of spicules. Unfortunately, our observation was before the launch of Hinode and we could not make use of the high-resolution images of SOT to compare.

3. Data Analysis

Dark subtraction and flat fielding were applied to the observed spectral images, then a mean sky spectrum was subtracted to obtain the proper emission profile of the spicules.

3.1. Method of Profile Fitting

We got the profiles at every pixel position along the slit between the hairlines in figure 2. The spacing is 0.15 arcsec per pixel, so we got about 650 profiles from each frame. Telluric lines were removed from the profiles, then each profile was fitted first with a single Gaussian curve as a function of wavelength from Hα line-center ($\Delta\lambda$), which determines relative peak intensity I_0, Doppler width $w_{\rm D}$, and Doppler shift $\Delta\lambda_{\rm D}$ of the emission.

$$I_{\rm single}(\Delta\lambda) = I_0 e^{-\left(\frac{\Delta\lambda-\Delta\lambda_{\rm D}}{w_{\rm D}}\right)^2} \tag{1}$$

Some profiles were asymmetrical and were not well fitted with a single Gaussian curve. The goodness of fit was eveluated by a reduced chi-square (χ^2) statistic. First we eliminated the low-intensity ($I_0 < 3.0$ sky brightness) profiles as they had a low signal-to-noise ratio. Then we introduced χ/I_0 as a threshold for a good fit, because the effect of the χ-values are influenced by intensity. For the profiles with a large χ/I_0 value, we tried to fit the observed profile with a sum of two Gaussian curves, and get two sets of parameters.

$$I_{\rm double}(\Delta\lambda) = I_{\rm slow} e^{-\left(\frac{\Delta\lambda-\Delta\lambda_{\rm slow}}{w_{\rm slow}}\right)^2} + I_{\rm fast} e^{-\left(\frac{\Delta\lambda-\Delta\lambda_{\rm fast}}{w_{\rm fast}}\right)^2} \tag{2}$$

The subscripts "slow" and "fast" denote the component with smaller and larger Doppler-shift values respectively.

Figure 4 is an example of a single-peaked and almost symmetrical profile which requires the double Gaussian fitting. While there remains substantial deviations at the peak and far wing of the profile in the case of the single Gaussian fitting (left panel), the double Gaussian fitting (right panel) can well follow the whole curve of the observed profile. The goodness of fit (chisq) becomes 10 times better in the case of the double Gaussian fitting. Similarly, for single-peaked but fairly asymmetrical profiles, the double Gaussian fitting works very well in our data.

All of the analyzed profiles are successfully fitted with single or double Gaussian curves. This confirms that the emissions in our selected frames were from optically thin part of the spicules.

3.2. Effect of Atmospheric Image Blurring

The spatial pattern of the spicule emission is blurred by the seeing effect. We tried to recover un-blurred spectral images with the help of 1-D Wiener filter method and checked the effect of atmospheric image blurring on the spectral parameters of emission profiles. We assumed that the point-spread-function (PSF) of the atmospheric blurring is a normal distribution. The width of the PSF was estimated from the smallest spatial width of observed emission and assumed to be uniform over the field of view. The power spectrum of the noise was estimated from the observed intensity fluctuation at the continuum wavelength domain where no spicular emissions were detected. Since its power spectrum was nearly flat, we assumed the noise to be white-noise.

An example of compensated spectral image is shown in figure 5 with its original observed image. We can see that the emission streaks became sharper in spatial direction and more clear in the "deconvolved" image.

The same spectral fitting method as described in the subsection 3.1 was applied to the deconvolved image to see the effect of atmospheric blurring on spectroscopic quantities. Figure 6 shows the results for two typical profiles. We can see that the spectral parameters do not change so much between the originally observed and the deconvolved image, except the intensity of the fast component. We performed the same comparison on all the profiles in the deconvolved spectral image, and estimated the effect of the atmospheric blurring on the spectroscopic parameters. For the single-Gaussian fitted profiles, I_0 changes less than ±5%, and $w_{\rm D}$ changes less than ±1%. The change of $\Delta\lambda_{\rm D}$ is smaller then 0.05 Å. In the case of asymmetric profiles, the changes of $w_{\rm slow}$ and $\Delta\lambda_{\rm slow}$ are also very small. $w_{\rm fast}$ changes ±8%, and $\Delta\lambda_{\rm fast}$ changes ±6%. $I_{\rm slow}$ decreases 4.5%, with 9.6% deviation. Only $I_{\rm fast}$ shows significant change, with average increase of about 14%. Increase in $I_{\rm fast}$ is expected since the deconvolution converges the blurring of isolated emission. Thus the spectroscopic parameters, especially the widths and the shifts of fitted components are not so influenced by the atmospheric blurring of the images.

Our method of seeing correction is based on a few assumptions, which are (1) the uniformity of seeing over the field of view, (2) whiteness of the power of background noise, etc. In the deconvolved image, there appear faint and equally-spaced emission streaks in the featureless part of the original spectral image. These equally-spaced emission patterns are probably artificial due to the drawback of the method we used. So we will proceed our discussion based on the analysis without the correction of atmospheric blurring.

4. Results

Line profiles of spicules can be grouped into three types. Profiles of the first type (Type A) can be fitted well with a single Gaussian curve. The second type (Type B) is not well fitted with single Gaussian, but it is nearly sym-

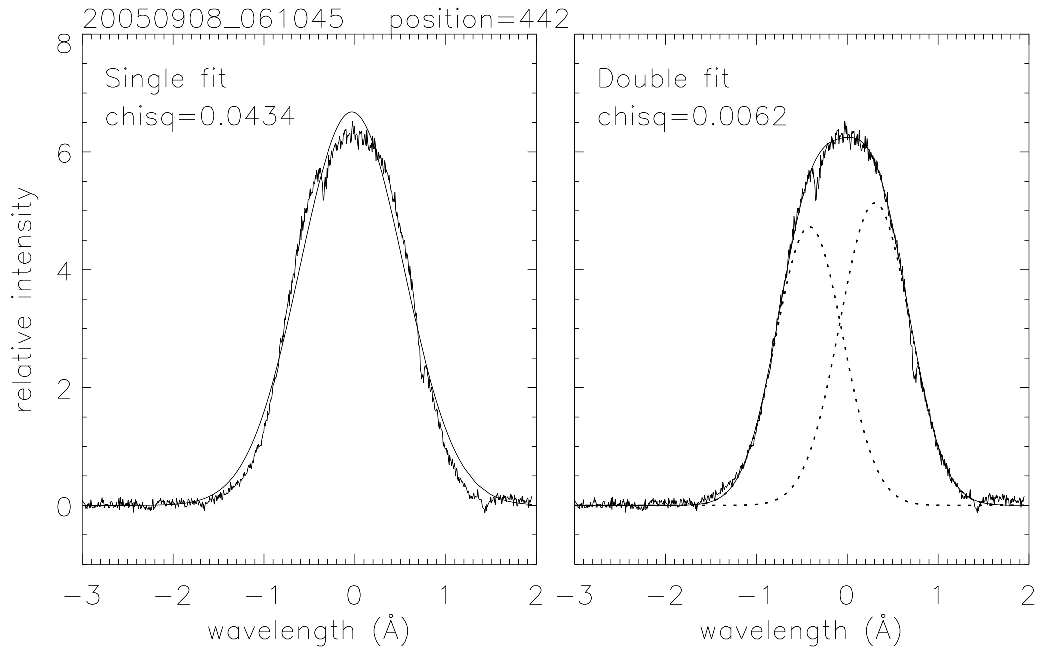

Fig. 4. Comparison of results with single and double Gaussian fitting. Though the original emission profile is almost symmetrical, single Gaussian fitting (left) cannot reproduce the observed profile. Double Gaussian fitting for the same profile (right) works well.

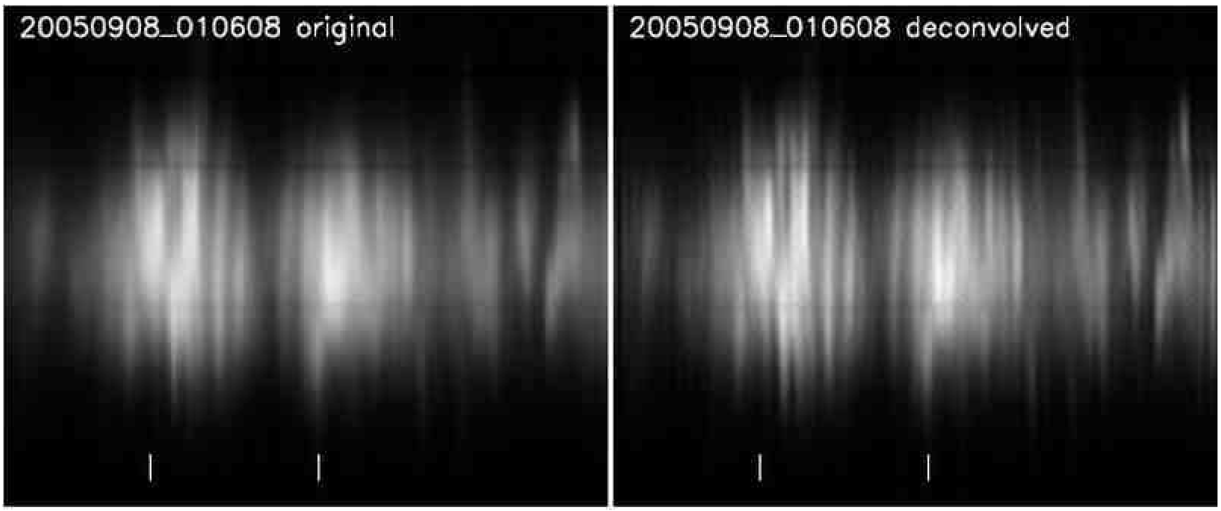

Fig. 5. The observed spectral image (left) and the processed image with the Wiener deconvolution method (right).

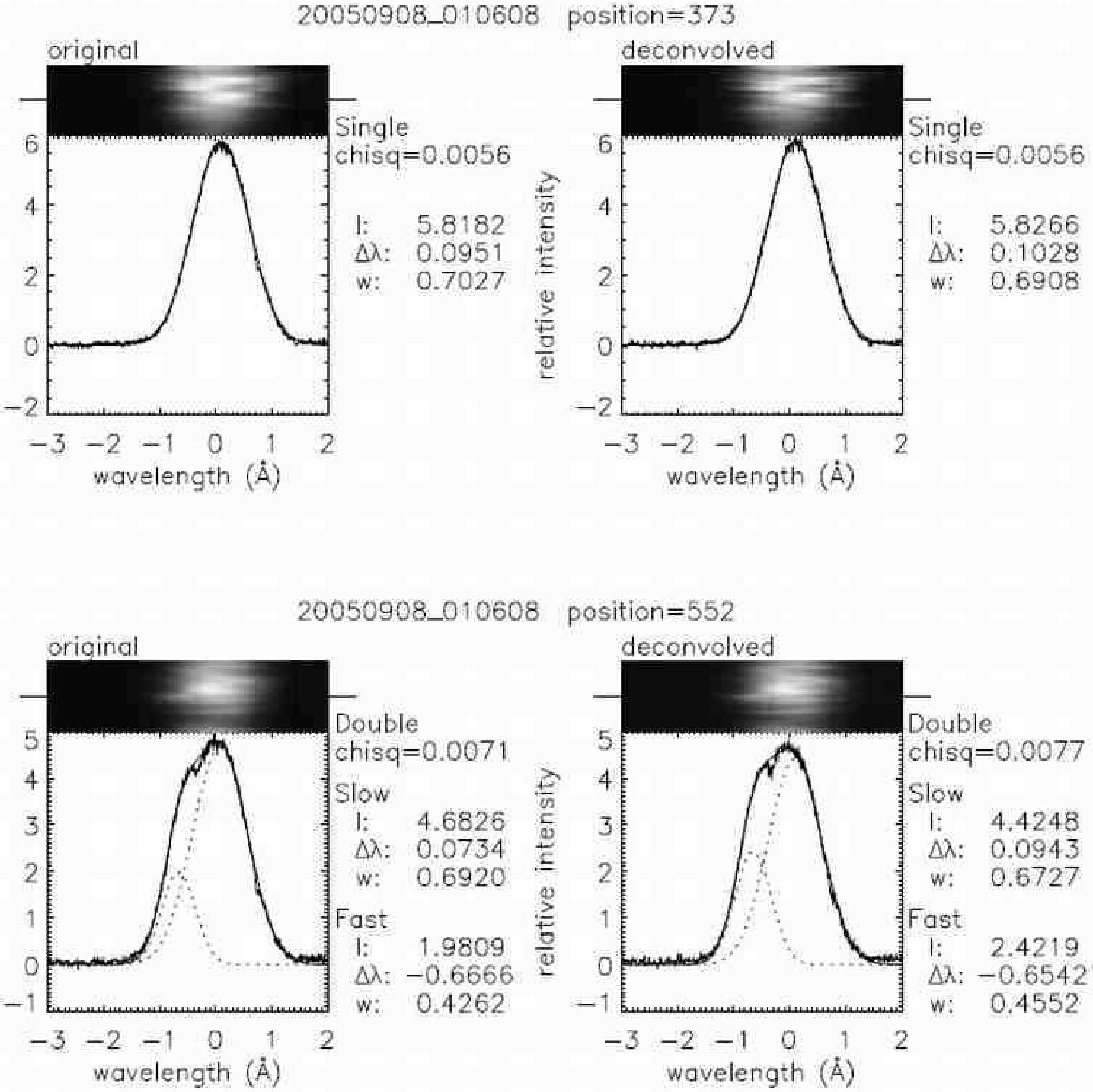

Fig. 6. Examples of the emission profiles to compare between the original and the "deconvolved" spectral images shown in figure 5.

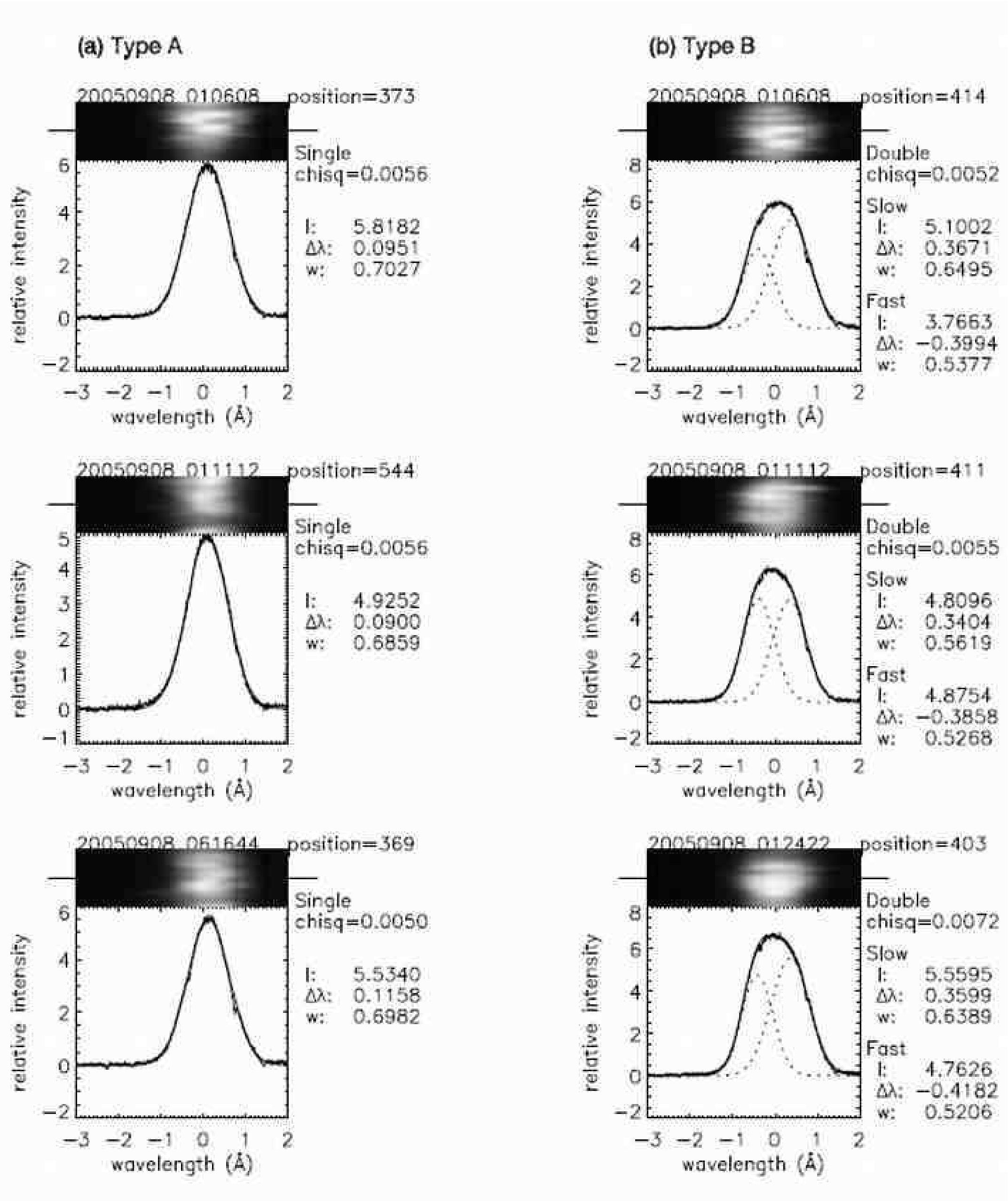

Fig. 7. Examples of the line profiles. The unit for wavelength shift ($\Delta\lambda$) and Doppler width (w) values is Å. (a) Typical Type A profiles, which are well fitted with a single Gaussian curve. (b) Typical Type B profiles, which are symmetrical, but cannot be fitted well with a single Gaussian curve.

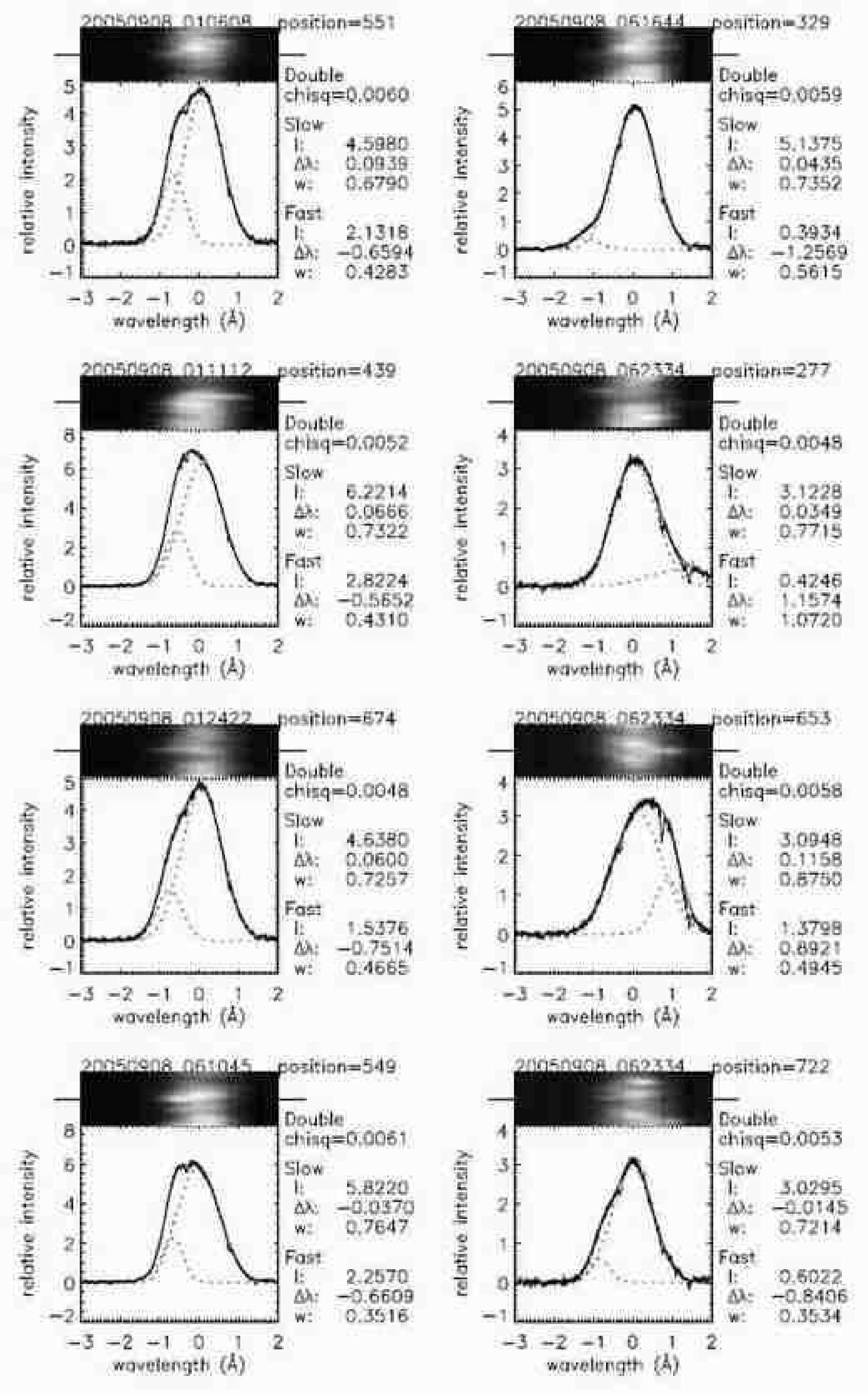

Fig. 8. Examples of the typical line profiles of Type C, which are asymmetrical and separated to slow and fast Gaussian components. The unit is the same as figure 7.

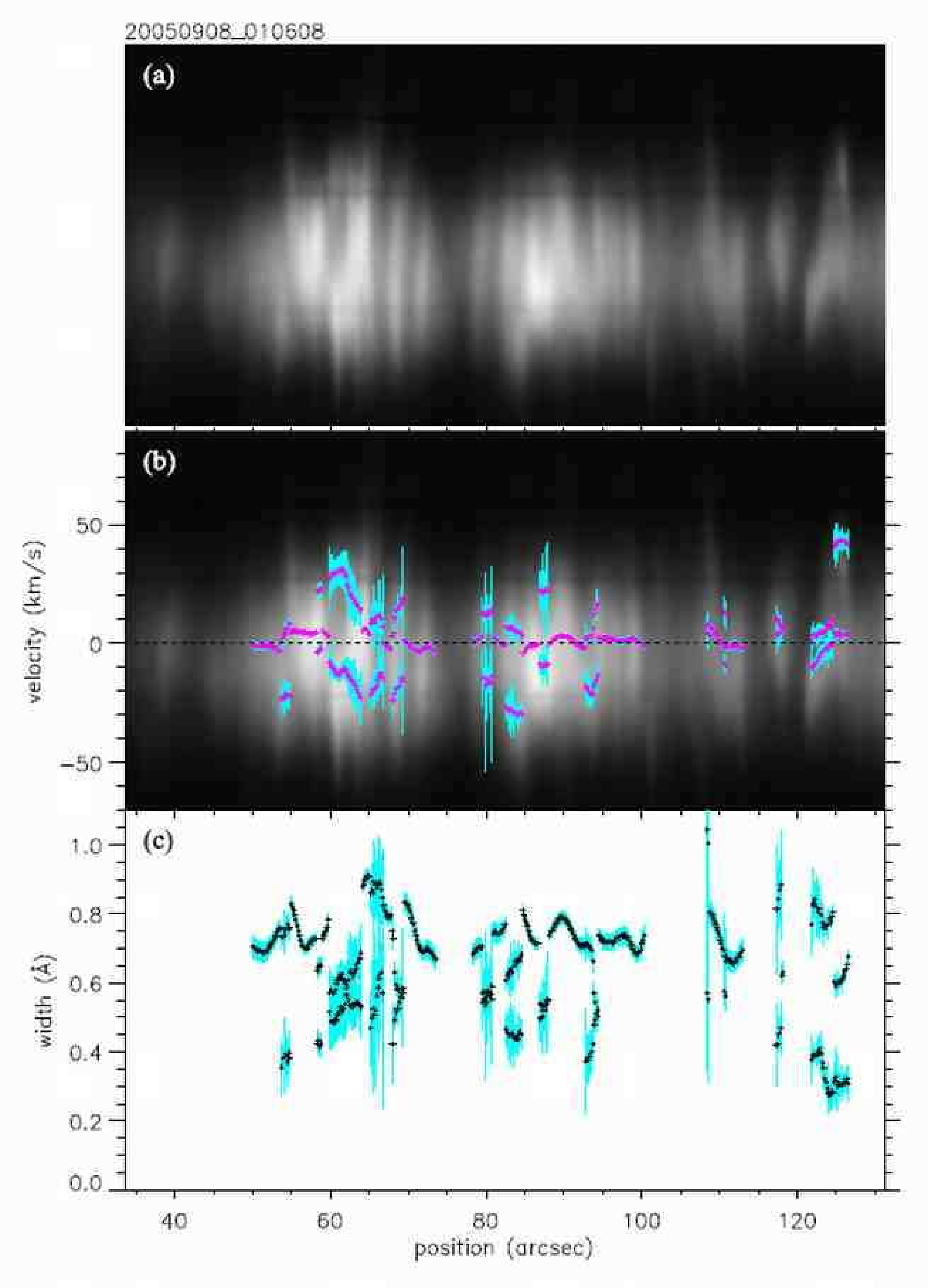

Fig. 9. (a) An example image showing Doppler shifted streaks of spicules. (b) Radial velocities determined by single or double Gaussian fitting are plotted over the same image as (a). Error bar (light blue) indicates the standard deviation of each velocity value. (c) Doppler widths of the profiles at the same positions as (b). Note that two values are plotted at the same axis position when the profile is fitted with double Gaussian curves.

Table 1. Classification of Hα profiles. Number of points where the line profile is categorized into three types are tabulated. Type A: well fitted with single Gaussian profile. Type B: ill fitted with single Gaussian, but almost symmetrical. Type C: asymmetrical profile which can be separated into slow and fast components.

Time (UT)	Type A	Type B	Type C
01:06:08	226	96	48
01:11:12	234	149	75
01:24:22	397	78	36
06:10:45	369	161	53
06:12:50	351	111	69
06:16:44	253	103	137
06:23:34	233	128	63
Total	2063 (61%)	826 (25%)	481 (14%)

metrical around the Hα line center (figure 4). The last type (Type C) is asymmetrical, and separated into an almost stationary component and a highly shifted component. Note that the difference between Types B and C is actually a matter of degree, and there are many profiles in-between. For argument's sake, we take the profiles with $|\Delta\lambda_{\rm fast}/\Delta\lambda_{\rm slow}| > 4.0$ as Type C and treat all other double Gaussian profiles as Type B. Figures 7 and 8 show the examples of typical profiles of each type, and table 1 lists the number of points categorized into each type.

Figure 9 is an example showing estimated LOS velocities and widths with the original spectral image. In figure 10, we summerize the distribution of Doppler widths, radial velocities, and equivalent widths in histogram format.

4.1. Doppler Width

Figure 10a shows that the Doppler widths of the Type A profile ($w_{\rm D}$) are 0.6–0.9 Å. Widths of the slow components of the Type C profile ($w_{\rm slow}$) are also 0.6–0.9 Å, while widths of the fast component ($w_{\rm fast}$) are 0.3–0.6 Å.

To identify the line-broadening mechanism, we calculated the theoretical Doppler width of Hα profile with given temperature T, microturbulence ξ, and macroturbulence Ξ,

$$w = \frac{\lambda}{c}\sqrt{\frac{2kT}{m} + \xi^2 + \Xi^2} \qquad (3)$$

where λ is the wavelength of Hα line, c is the light velocity, k is Boltzmann constant, and m is hydrogen mass.

The result is shown in figure 11. When $\Xi = 0$, the observed value $w_{\rm fast} = 0.35$ Å is found within a reasonable range of temperature and microturbulence, $T \simeq 15000$ K and $\xi \simeq 5$ km s^{-1}. On the other hand, even if we assume as high a temperature as $T = 20000$ K with microturbulence $\xi = 20$ km s^{-1} we cannot get a width more than 0.6 Å. While Beckers (1972) listed the most likely temperature as 9000–16000 K, Makita (2003) derived ionization temperature for hydrogen to be 5200 K and excitation temperature for Hα to be 5020 K, and other authors also reported lower temperatures. Therefore, it is unlikely that the tempetrature of spicules to be higher than 20000 K. And considering that microturbulent velocity cannot be

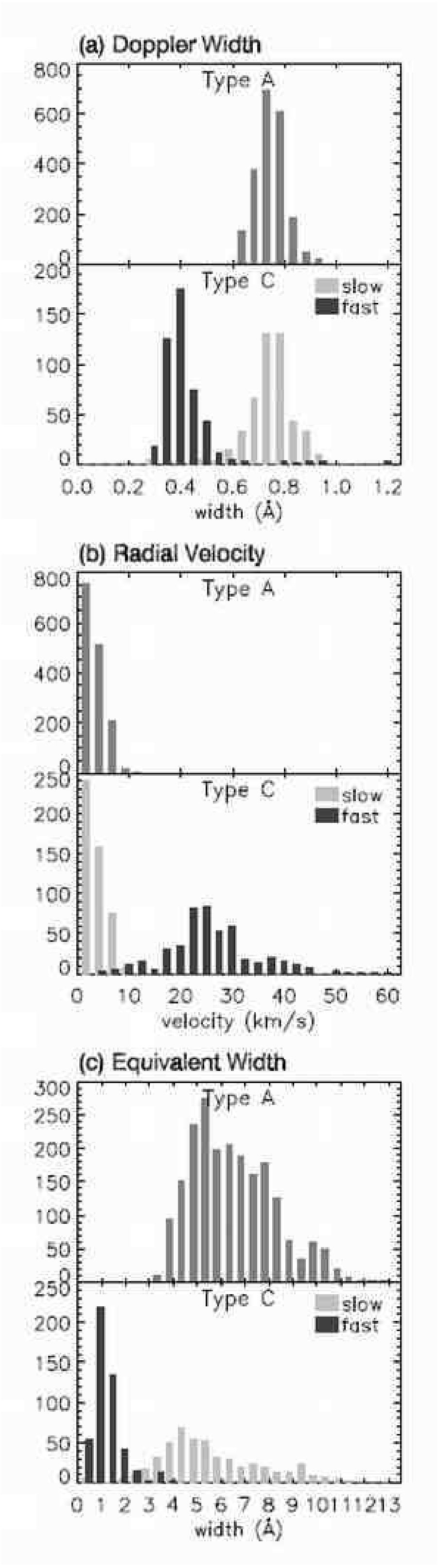

Fig. 10. Histograms made from the results of all frames. "Slow" and "fast" mean the slow and the fast components of the Type C profile. (a) Doppler width. (b) Radial velocity (absolute value). (c) Equivalent width.

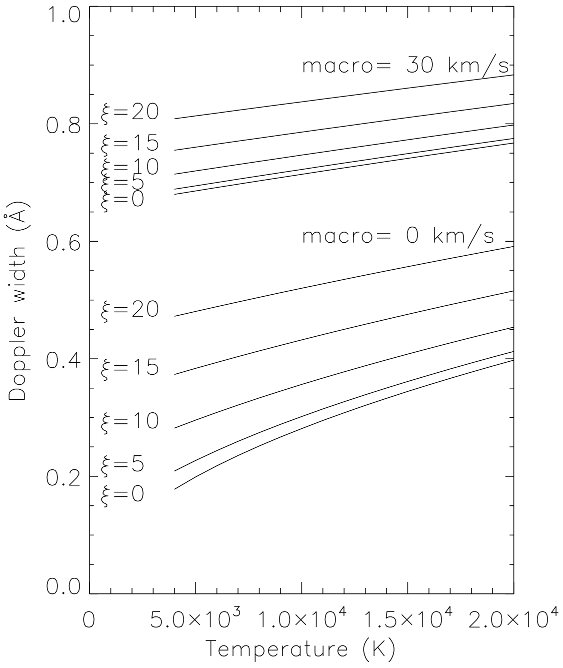

Fig. 11. Theoretical Doppler width, calculated as a function of temperature with different values of microturbulent velocity ξ (km s^{-1}) and macroturbulent velocity.

supersonic, we need additional "macroturbulence" to explain the observed $w_{\rm slow}$ and $w_{\rm D}$.

From figure 11, we find that the required Ξ for $w_{\rm slow}$ and $w_{\rm D}$ is about 30 km s^{-1}. Here we use the term "macroturbulence" to include any non-thermal random velocities other than microscopic turbulence. There exists many spicules with various LOS velocities along the LOS of observation. Superposition of their emissions will result in the broadening of the observed profile. "Macroturbulent velocity" is a measure of the dispersion of their LOS velocities.

4.2. Radial Velocity

Figure 10b is the histogram of radial (line-of sight) velocities. With our definition for Type C, the distribution of the fast component's parameters hardly overlaps with that of the slow component's. Radial velocities derived from Type A profiles are less than 10 km s^{-1}, and the profiles of the slow component of Type C give similar values. The distribution of the fast component peaks at around 25 km s^{-1} and there is also a small peak at around 40 km s^{-1}.

4.3. Correlation between Width and Velocity

Figure 12 is a correlation plot between radial velocities and Doppler widths for Types A and C. Again, it is clear that the slow component of the Type C profile has a similar distribution to the Type A profile. The velocity of the fast component spreads from 10 km s^{-1} to 40 km s^{-1}, but its width is independent of radial velocity.

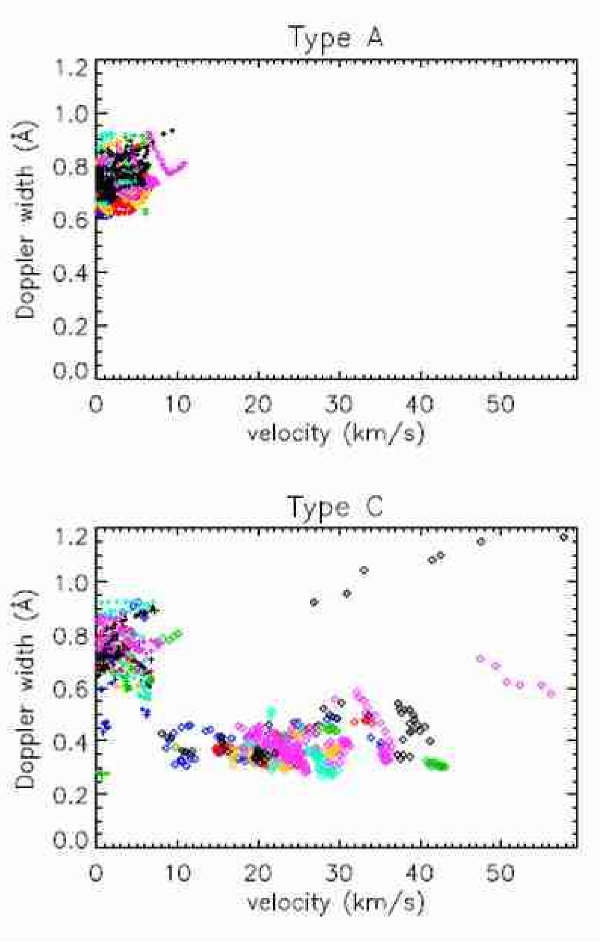

Fig. 12. Correlation between velocity (absolute value) and Doppler width. Crosses are for the slower component and diamonds are for the faster component. Different color represents different time.

5. Summary and Discussion

We made high-resolution spectroscopic observations of limb spicules in Hα. While more than half of the observed spicules have Gaussian line profiles (Type A), some spicules have distinctly asymmetric profiles which can be fitted with two Gaussian components (Type C). The faster component of Type C profiles have radial velocities of 10–40 km s^{-1} and Doppler width of $\sim$0.4 Å. This width can be explained with temperature $\simeq$15000 K and microturbulence $\simeq$5 km s^{-1}. On the other hand, widths of Type A profiles and the slower component of Type C profiles are 0.6–0.9 Å. Macroturbulent velocities of order 30 km s^{-1} are required to explain this large width.

Now we will discuss the physical interpretations of these results.

Figure 2 shows that the slit-line intersects many spicules, and it is natural that the LOS intersects several spicules, too. Though it is difficult to observe a single spicule without superposition of other spicules, Type C profile enables us to separate the emission of single spicule as the fast component of double-Gaussian fitted components. Line width of the fast component can be explained with temperature $\simeq$15000 K and microturbulence $\simeq$5 km s^{-1}. Broad width of the Type A profiles suggest that many spicules along the LOS contribute to the observed emission. Figure 10c shows that their equivalent widths are five times or more larger than those of the fast component.

The LOS velocity 20–40 km s^{-1} of the fast component is consistent with the velocity of the apparent up-and-down motion of spicules reported by many authors (e.g. Nishikawa 1988; De Pontieu et al. 2007b; Pasachoff, Jacobson, Sterling 2009). Because most spicules are nearly vertical to the solar limb (Beckers 1972), their LOS velocities are much smaller than their actual velocities. We suppose that the profiles of Type A and slow component of Type C are from these nearly vertical spicules, and that the fast component is from the few spicules which are almost parallel to the LOS.

As shown in section 4.1, we need additional macroturbulent i.e. non-thermal random velocities of order 30 km s^{-1} to explain the Doppler width of the slow component of Type C and the Type A profiles. Other observations also reported the high non-thermal broadening. For example, Makita (2003) suggested that spicules have a turbulence of $\sim$20 km s^{-1} in the active region, based on the analysis of Ca II H and K profiles in the flash spectrum of the 1958 eclipse. And Mariska, Feldman, Doschek (1978) reported average non-thermal velocity of 28 km s^{-1} in EUV line profiles at the quiet limb. Next we proceed to discuss the source of macroturbulence.

One of the possible sources is ejecting motion of spicules inclined toward or away from the observer. Variations in speed and inclination of ejection produce the dispersion of LOS velocities. As discussed above, most spicules have small inclinations and so their LOS velocities will be much smaller than 10–40 km s^{-1}. Distributions of apparent inclinations reported by Pasachoff, Jacobson, Sterling (2009) have peaks at 10 and 25 degrees, in which case the LOS velocity of ejection speed 40 km s^{-1} will be at most 7 and 17 km s^{-1}. They are too small to explain the observed widths. There is also the height difference of ejection speed. The spicules nearer to us or farther than the limb of the sun would be observed in superposition against lower heights of spicules whose bases are on the limb. However, the speed at the tops is no faster than the lower part (Sterling 1998; De Pontieu et al. 2007b), and it will contribute little to the line broadening, similar to the argument above.

Another possible source is the lateral motion of spicules due to the Alfvén wave disturbance recently found in Hinode/SOT Ca II H filtergrams (De Pontieu et al. 2007a; Suematsu et al. 2008; He et al. 2009b), or the kink wave observed by He et al. (2009a). De Pontieu et al. (2007a) showed that the distribution of transverse displacements of the spicules agrees with the velocity amplitudes around 20 km s^{-1}, while He et al. (2009b) reported the velocity amplitude of high-frequency Alfvén waves to be 4.7–20.8 km s^{-1}. Velocity amplitude of the kink wave reported by He et al. (2009a) is less than 8 km s^{-1}. Superposition effects of these motions can broaden the line profiles. Because spicules are believed to be ejected along magnetic field lines, transverse Alfvén waves broaden the Hα line profiles of Type A or slow component of Type C. MHD simulation also showed that the amplitude of Alfvén waves at the chromospheric height to be $\sim$20 km s^{-1} (Suzuki & Inutsuka 2006). However, when the sinusoidal motions of independently disturbed spicules are superposed, its standard deviation will be $1/\sqrt{2}$ of amplitude. Thus oscillation of velocity amplitude 20 km s^{-1} will contribute only 14 km s^{-1} to the macroturbulent velocity. As for the fast components, we assume that their surrounding magnetic field is nearly parallel to the LOS, so the Alfvén waves will not contribute to line-broadening, agreeing with their narrow widths even if they are composed of multiple finer threads. Kulidzanishvili (1980) reported the oscillations of the radial velocities of limb spicules with the period of 3–7 min. However, their amplitudes were less than 10 km s^{-1}, which are too small to contribute to our observed line-widths.

Even when we include superposition effects of ejecting motions and Alfvén wave broadening, it is still insufficient to explain the macroturbulent velocities of $\sim$30 km s^{-1}. So there must be some additional but unidentified sources for the non-thermal broadening of spicule emission profiles. Alfvén waves with higher frequencies and shorter wavelengths than those observed until now may be present and contribute to the broadening.

Let us mention two interesting events found in our analysis. Their characteristics are different from the common spicules discussed so far. While most of radial velocities are less than 40 km s^{-1}, these two cases have much larger (> 45 km s^{-1}) radial velocities as seen in the upper right area of figure 12. Their Doppler widths are exceptionally large, too. They are in the spectra at 06:16:44 UT and 06:23:34 UT, and their faint and broad profiles can be found in figure 8. The positions of these events are marked in figure 2 where there is a gap in the bush of spicules, and where the slit is the nearest to the limb. We need different broadening mechanism for these events. It may be an event with a magnetic reconnection, or something related to the spicule formation. This phenomenon may correspond to the Type II spicules of De Pontieu et al. (2007b) or to macrospicules (Bohlin et al. 1975; Yamauchi et al. 2003) or to polar-jets (Shibata et al. 1992; Shimojo et al. 1996; Savcheva et al. 2007). The relations are yet to be ascertained in future studies.

In this paper, we treated the results statistically without regard to their positions. However, figure 3 shows that some spicules appear as tilted streaks. This is possibly an evidence of rotation of spicules suggested by Pasachoff, Noyes, Beckers (1968), and its spatially blurred emission may contribulte to broaden the line profiles.

Some physical values are not determined by the Hα profile alone. In order to study the true origin of macroturbulence or of the high-velocity events, we need simultaneous spectroscopic observations of spicules in multiple spectral lines, which can be achieved with the Horizontal Spectrograph at Hida Observatory. We also need high spatial-resolution images of Hinode/SOT simultaneously obtained with the spectroscopic observation to understand the details of spicules. We will plan our next observation to accommodate to those requirements.

We thank the referees for the greatly helpful comments. We are grateful for the use of EIT data obtained on the SOHO spacecraft. SOHO is a project of international cooperation between ESA and NASA. The authors are supported by a grant-in-aid for the Global COE program "The Next Generation of Physics, Spun from Universality and Emergence" from the Ministry of Education, Culture, Sports, Science and Technology (MEXT) of Japan, and by the grant-in-aid for "Creative Scientific Research The Basic Study of Space Weather Prediction" (17GS0208, PI: K. Shibata) from the Ministry of Education, Culture, Sports, Science and Technology of Japan, and also partly supported by the grant-in-aid from the Ministry of Education, Culture, Sports, Science and Technology of Japan (No.19540474).

References

Beckers, J. M. 1972, ARA&A, 10, 73

Bohlin, J. D., Vogel, S. N., Purcell, J. D., Sheeley, N. R., Jr., Tousey, R., & Vanhoosier, M. E. 1975, ApJ, 197, L133

De Pontieu, B., et al. 2007a, Science, 318, 1574

De Pontieu, B., et al. 2007b, PASJ, 59, S655

Hasan, S. S., & Keil, S. L. 1984, ApJ, 283, L75

He, J., Marsch, E., Tu, C., & Tian, H. 2009b, ApJ, 705, L217

He, J., Tu, C., Marsch, E., Guo, L., Yao, S., & Tian, H. 2009a, A&A, 497, 525

Krat, V. A., & Krat, T. V. 1971, Sol. Phys., 17, 355

Kulidzanishvili, V. I. 1980, Sol. Phys., 66, 251

Kulidzanishvili, V. I., & Nikolsky, G. M. 1978, Sol. Phys., 59, 21

Makita, M. 2003, Publ. Nat. Astr. Obs., 7, 1

Mariska, J. T., Feldman, U., & Doschek, G. A. 1978, ApJ, 226, 698

Nishikawa, T. 1988, PASJ, 40, 613

Pasachoff, J. M., Jacobson, W. A., & Sterling, A. C. 2009, Sol. Phys., 260, 59

Pasachoff, J. M., Noyes, R., & Beckers, J. M. 1968, Sol. Phys., 5, 131

Savcheva, A., et al. 2007, PASJ, 59, S771

Shibata, K. 1992, PASJ, 44, L173

Shimojo, M., Hashimoto, S., Shibata, K., Hirayama, T., Hudson, H., & Acton, L. 1996, PASJ, 48, 123

Sterling, A. C. 1998, in Proc. Solar Jets and Coronal Plumes, ESA, SP-421, 35

Suematsu, Y., Ichimoto, K., Katsukawa, Y., Shimizu, T., Okamoto, T., Tsuneta, S., Tarbell, T., & Shine, R.A. 2008, in ASP Conference Ser., 397, First Results From Hinode, ed. S.A. Matthews, J.M. Davis and L.K. Harra (San Francisco: ASP), 27

Suzuki, T. K., & Inutsuka, S., 2006, J. Geophys. Res., 111, A06101

Yamauchi, Y., Moore, R. L., Suess, S. T., Wang, H., & Sakurai, T. 2003, BAAS, 35, 812